First-principles study of point defects in $LiGaO_2$

Adisak Boonchun,[1,2] Klichchupong Dabsamut,[1,2] and Walter R. L. Lambrecht[3,a)]
[1)] *Department of Physics, Faculty of Science. Kasetsart University, Bangkok 10900 Thailand*
[2)] *Thailand Center of Excellence in Physics, Commission on the Higher Education, Bangkok 10400, Thailand*
[3)] *Department of Physics, Case Western Reserve University, 10900 Euclid Avenue, Cleveland, Ohio 44106-7079, USA*

The native point defects are studied in $LiGaO_2$ using hybrid functional calculations. We find that the relative energy of formation of the cation vacancies and the cation antisite defects depends strongly on the chemical potential conditions. The lowest energy defect is found to be the Ga_{Li}^{2+} donor. It is compensated mostly by V_{Li}^{-1} and in part by Li_{Ga}^{-2} in the more Li-rich conditions. The equilibrium carrier concentrations are found to be negligible because the Fermi level is pinned deep in the gap and this is consistent with insulating behavior in pure $LiGaO_2$. The V_{Ga} has high energy under all reasonable conditions. Both the Ga_{Li} and the V_O are found to be negative U centers with deep $2+/0$ transition levels.

I. INTRODUCTION

Recently, there has been an interest in ultra-wide-band-gap semiconductors such as β-Ga_2O_3 because of their potential in pushing high-power transistors to the next level of performance.[1,2] An important figure of merit for such applications is the breakdown field and the latter is directly correlated with the band gap. Here we draw attention to an even higher band gap material, $LiGaO_2$. $LiGaO_2$ has a wurtzite-derived crystal structure[3,4] and band gap of ∼5.3-5.6 eV (at room temperature) based on optical absorption[5–8]. A theoretical value of 6.25 eV (at $T = 0$) based on quasi-particle self-consistent (QS) GW calculations,[9] with G the one-particle Green's function and W the screened Coulomb potential, may be an overestimate due to insufficient k-point sampling. It can be thought of as a I-III-VI_2 ternary analog of wurtzite ZnO, in which each group II Zn atom is replaced by either a group-I Li or a group III-Ga in a specific ordered pattern with the $Pna2_1$ spacegroup. In this structure the octet rule is satisfied because each O is surrounded tetrahedrally by two Li and two Ga. The prototype for this crystal structure is β-$NaFeO_2$. $LiGaO_2$ can be grown in bulk form by the Czochralsky method[3] and because of its good lattice match has been explored as a substrate for GaN. It can also be grown by epitaxial methods on ZnO and vice versa. Mixed ZnO-$LiGaO_2$ alloys have been reported.[10,11] It has been considered for piezoelectric properties,[12–14] and is naturally considered as a wide gap insulator. However, Boonchun and Lambrecht[15] suggested it might be worthwhile considering as a semiconductor electronic material and showed in particular that it could possibly be n-type doped by Ge. That study only used the 16 atom primitive unit cell of $LiGaO_2$ and thus considered rather high (25 %) Ge_{Ga} doping or Mg_{Li} doping. It did not study the site competition or native defect compensation issues. Here we study the native point defects by means of hybrid functional supercell calculations.

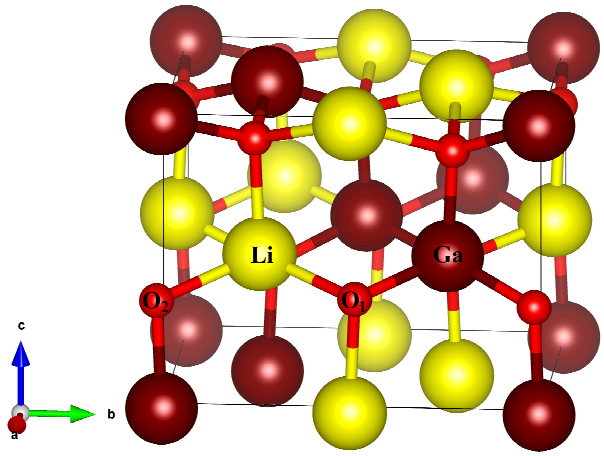

FIG. 1. Crystal structure of $LiGaO_2$ in the $Pna2_1$ space-group.

II. COMPUTATIONAL METHOD

Our study is based on density functional calculations using the Heyd-Scuseria-Ernzerhof (HSE) hybrid functional.[16,17] The calculations are performed using the Vienna Ab-Initio Simulation Package (VASP).[18,19] The electron ion interactions are described by means of the Projector Augmented Wave (PAW) method.[20,21] We use a well-converged energy cut-off of 500 eV for the projector augmented plane waves.

The lattice constants and reduced coordinates of the perfect crystal in the $Pna2_1$ (No. 33) space group were fully optimized and agree well with Ref. 14. This orthorhombic structure is closely related to wurtzite with $a \approx a_w\sqrt{3}$, $b_o = 2a_w$, and $c_o = c_w$ with subscripts o indicating orthorhombic and w wurtzite. The crystal structure is shown in Fig. 1. We performed the calculations for the defects with a supercell size of 128 atoms (which corresponds to $2 \times 2 \times 2$ the primitive unit cell) and a single **k**-point shifted away from Γ is employed for the Brillouin zone integration. The supercell is large enough that a single **k**-point sampling is sufficient. By choosing

a)Electronic mail: walter.lambrecht@case.edu

it away from Γ the best accuracy is achieved for a single point sampling at the slightly extra cost that the wave functions are complex instead of real. A convergence test for the V_O showed that the energy of formation was lowered by 0.02 eV in the neutral charge state when using a $2 \times 2 \times 2$ mesh instead of the single-point mesh and the 0/2+ transition state also shifted down by only 0.01 eV. These changes are within the expected error bar. The lattice constants of the supercell are kept fixed to those of the perfect crystal because we intend to represent the dilute limit in which a defect will not affect the volume of the overall crystal. The atomic positions in the defect containing supercells are fully relaxed. The valence configurations used were $2s^1$ for Li, $3d^{10}4s^24p^1$ for Ga and $2s^22p^4$ for O. In the HSE functional, the Coulomb potential in the exchange energy is divided into short-range and long-range parts with a screening length of 10 Å and only the short-range part of the exact Hartree-Fock non-local exchange is included by mixing it with the generalized gradient Perdew-Burke-Enrzerhof (PBE) potential with a mixing fraction $\alpha = 0.25$. The band gap obtained in this way ($E_g = 5.10$ eV) is slightly lower than the experimental value of 5.3-5.6 eV.

The analysis of the defect levels follows the standard defect approach as outlined in *e.g.* Freysoldt *et al.*[22] The energy of formation of the defect D^q in charge state q is the key quantity obtained from the calculation and is given by

$$E_f(D^q) = E_{tot}(C:D^q) - E_{tot}(C) - \sum_i \Delta n_i \mu_i + q(\epsilon_v + \epsilon_F + V_{align}) + E_{cor} \quad (1)$$

where $E_{tot}(C:D^q)$ is the total energy of the supercell containing the defect and $E_{tot}(C)$ is the total energy of the perfect crystal supercell. The chemical potentials μ_i represent the energy for adding or removing atoms from the crystal to a reservoir in the process of making the defect. The Δn_i is the change in number of atoms of species i. Likewise the chemical potential of the electron determining its charge state is $\epsilon_F + \epsilon_v + V_{align}$ with ϵ_v the energy of an electron at the valence band maximum (VBM) relative to the average electrostatic potential in bulk and ϵ_F the Fermi energy in the gap measured from the VBM. The alignment potential V_{align} represents the alignment of the average electrostatic potential in the supercell far away from the defect relative to that in the bulk. This is calculated using the Freysoldt *et al.* approach.[22,23] The final term is the image charge correction term which corrects for the Madelung energy of the periodic array of net defect point charges in the uniform background that is added to ensure overall charge neutrality when considering a locally charged defect state. It is closely related to the alignment potential and including these corrections allows one to extrapolate the energy of formation to the dilute limit of an infinitely large supercell. The defect level occupations are kept fixed for a given charge state automatically by our single **k**-point sampling, which avoids metallic partial occupation of the defect bands of the supercell.

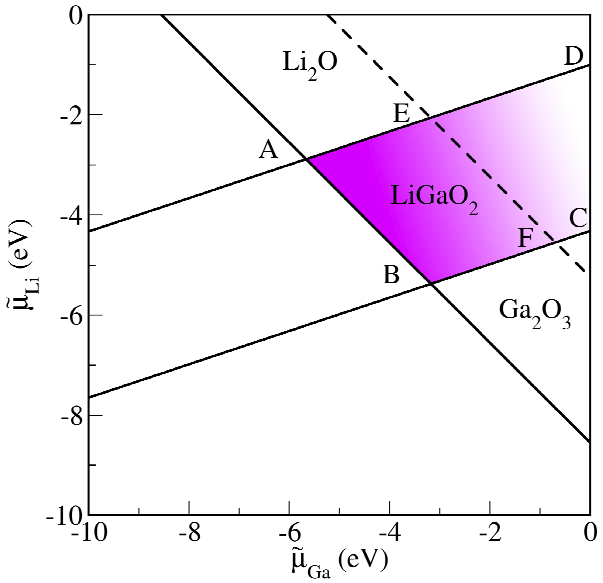

FIG. 2. Chemical potential phase diagram, showing the region of stability of $LiGaO_2$ in terms of the excess chemical potentials.

III. RESULTS

First, to check the accuracy of our calculations for the perfect crystal, we give the optimized lattice constants obtained in hybrid functional compared to experiment and previous results in Table I. The reduced coordinates are also given and agree well with previous work.[14] One can see that the HSE agrees with experiment better than the LDA. The lattice constants only slightly (0.1%) overestimate experiment while LDA underestimated them by ~ 1.2 %.

TABLE I. Calculated lattice constant and reduced coordinate of $LiGaO_2$ compared to experimental data.

Lattice constant (Å)	Method	a	b	c
Present calculation	HSE	5.407	6.369	5.027
Previous work[14]	LDA	5.361	6.255	4.953
Experimental data[3]		5.402	6.372	5.007
Reduced Coordinate	Atom	x	y	z
HSE Calculation	Ga	0.0817	0.1261	0
	O_1	0.4072	0.1386	0.8918
	O_2	0.0689	0.1125	0.3682
	Li	0.4177	0.1245	0.4960
Experimental data[3]	Ga	0.0821	0.1263	0
	O_1	0.4066	0.1388	0.8927
	O_2	0.0697	0.1121	0.3708
	Li	0.4207	0.1267	0.4936

Next, we discuss the chemical potentials used in the

defect calculation formation energies. The chemical potentials $\mu_i = \mu_i^0 + \tilde{\mu}_i$, where μ_i^0 are the chemical potentials of each species in its reference state, namely the phase it occurs in at standard pressure and room temperature, and $\tilde{\mu}_i$ are the excess chemical potentials. The latter are viewed as a tunable parameter reflecting the growth conditions but must obey certain restrictions based on thermodynamic equilibrium. These include

$$\tilde{\mu}_{\rm Li} + \tilde{\mu}_{\rm Ga} + 2\tilde{\mu}_O = \tilde{\mu}_{\rm LiGaO_2} \quad (2)$$

where $\tilde{\mu}_{\rm LiGaO_2}$ is the energy of formation of $LiGaO_2$, which we calculated to be -8.55 eV. Each of the excess chemical potentials $\tilde{\mu}_i \leq 0$ on the left must be less than zero in order to avoid precipitation of the bulk elements Li and Ga or evolving O_2 gas. For example, $\mu_{\rm Li}^0$ corresponds to metallic body-centered-cubic Li and thus $\tilde{\mu}_{\rm Li} = 0$ corresponds to the assumption that the crystal with the defect is in equilibrium with bulk metallic Li as reservoir. Similarly $\tilde{\mu}_{\rm Ga} = 0$ corresponds to equilibrium with metallic bulk Ga and $\tilde{\mu}_{\rm O}$ corresponds to O in the O_2 molecule. The $\mu_{\rm O}$ corresponds to the total energy of oxygen in an isolated O_2 molecule for which we find the value $\mu_{\rm O} = \frac{1}{2}E_{tot}[{\rm O_2}]$ = -6.99 eV in HSE. Our calculated binding energy $E_{tot}[{\rm O_2}] - 2{\rm E_{tot}[O]}$ is -5.17 eV, compared to -5.12 as experimental value.[24] However, we need to also consider further restrictions imposed by competing binary compounds β-Ga_2O_3 and Li_2O.

$$\begin{aligned} 2\tilde{\mu}_{\rm Li} + \tilde{\mu}_{\rm O} &\leq \tilde{\mu}_{\rm Li_2O}, \\ 2\tilde{\mu}_{\rm Ga} + 3\tilde{\mu}_{\rm O} &\leq \tilde{\mu}_{\rm Ga_2O_3}. \end{aligned} \quad (3)$$

These restrictions determine the region of chemical potentials in which $LiGaO_2$ is stable relative to the competing binaries and elements. They are bounded by

$$\begin{aligned} \tilde{\mu}_{\rm Li} &\geq \frac{1}{3}\tilde{\mu}_{\rm Ga} + [\tilde{\mu}_{\rm LiGaO_2} - \frac{2}{3}\tilde{\mu}_{\rm Ga_2O_3}], \\ \tilde{\mu}_{\rm Li} &\leq \frac{1}{3}\tilde{\mu}_{\rm Ga} + \frac{1}{3}[2\tilde{\mu}_{\rm Li_2O} - \tilde{\mu}_{\rm LiGaO_2}]. \end{aligned} \quad (4)$$

with $\tilde{\mu}_{\rm LiGaO_2} - \frac{2}{3}\tilde{\mu}_{\rm Ga_2O_3} = -4.32$ eV and $\frac{1}{3}[2\tilde{\mu}_{\rm Li_2O} - \tilde{\mu}_{\rm LiGaO_2}] = -1.00$ eV.

It is represented in the phase diagram shown in Fig. 2. The points A, B, C, D correspond respectively to (A) Li-rich, Ga-poor, (B) Li-poor as well as relative Ga-poor, (C) Ga-rich, Li-poor and (D) Ga-rich and Li-rich but O-poor. The shading of the color is darker the higher the chemical potential of O and the line AB corresponds to the O-rich limit $\tilde{\mu}_{\rm O} = 0$. In addition to the extreme chemical potential conditions (Ga-rich and Li-rich), we consider an intermediate oxygen chemical potential corresponding to a realistic growth condition during the annealing of $LiGaO_2$. The oxygen chemical potential is a function of temperature and oxygen partial pressure, as described by Reuter *et al.*[25]

$$\tilde{\mu}_{\rm O}(T,p) = \tilde{\mu}_{\rm O}(T,p_0) + \frac{1}{2}k_B T \ln(p/p_0), \quad (5)$$

where $\tilde{\mu}_{\rm O}(T,p_0)$ is the oxygen chemical potential at the standard pressure $p_0 = 1$ atm, k_B is Boltzmann's constant, and T is the temperature in Kelvin. In the growth experiment of Ref. 8, the mixed Li_2CO_3 and Ga_2O_3 powders were compressed into tablets and then calcined at 1200 °C for 20 h in air.[8] We therefore choose an annealing temperature of 1200°C and an oxygen partial pressure of 0.21 atm which represents the ratio of oxygen gas in ambient environment. The growth conditions at annealing temperature of 1200 °C and oxygen partial pressure of 0.21 atm is represented by the dashed line EF in Fig. 1.

The defects considered are the vacancies $V_{\rm Ga}$, $V_{\rm Li}$ and $V_{\rm O}$ and the antisites $\rm Li_{Ga}$ and $\rm Ga_{Li}$. The effects of spin polarization were included for cases with unpaired electrons in defect levels. Interstitial defects will be considered in the future but comparison with II-IV-N_2 semiconductors suggest that they would be of high energy.[26,27] The defect energies of formation are shown for the six chemical potential points A, B, C, D, E and F in Fig. 3.

First we see that $\rm Ga_{Li}$ is the lowest energy defect for $\epsilon_F = 0$ in all cases. It is a double donor, which is in the 2+ charge state over most of the gap. Still, it has a well-defined $2+/0$ transition making it a negative U system. In Fig. 4 we can see that while for the neutral charge state, the O around $\rm Ga_{Li}$ move outward, they move inward for the 2+ charge state with an in-between outward relaxation for the 1+ state. The additional stabilization by outward motion of the O when adding two electrons rather than one causes the negative U behavior where the 1+ charge state is never the lowest energy one for any Fermi level position. It is thus not behaving like a simple shallow donor, consistent with the relatively deep donor binding energy of 0.74 eV below the conduction band minimum (CBM). We thus do not expect it to be an effective n-type dopant. We can see that this defect has negative energy of formation at $\epsilon_F = 0$ in most cases. This reflects that even in the most Ga-poor case, this defect is hard to avoid because we cannot make the system poor enough in Ga without reaching the stability limit imposed by Li_2O. On the other hand, a Fermi level $\epsilon_F = 0$ is not expected to be realistic as discussed later.

The $\rm Li_{Ga}$ antisite on the other hand is a double acceptor which can occur in $0, -1, -2$ charge states. It is the lowest energy defect in its -2 charge state near the CBM in cases A, D and E. These are the cases richest in Li.

As for the vacancies, $V_{\rm Li}$ occurs in $0, -1$ charge states, while $V_{\rm Ga}$ occurs in $0, -1, -2, -3$ charge states. We can see that $V_{\rm Ga}^0$ has a high energy of formation in all cases. Although its negative charge states have significantly lower energy for ϵ_F close to the CBM, it never becomes the lowest energy defect and therefore does not play a major role in determining the Fermi level. The $V_{\rm Li}$ is more interesting. Although it has high energy in the Li-rich case D (which is somewhat unrealistic and O-poor) it has low energy in the Li-poor cases, B, C, F. Even in case E, its intersection with the $\rm Ga_{Li}^{2+}$ occurs close to that of the intersection of the latter with $\rm Li_{Ga}^{2-}$. We thus expect that both these acceptors may play a role

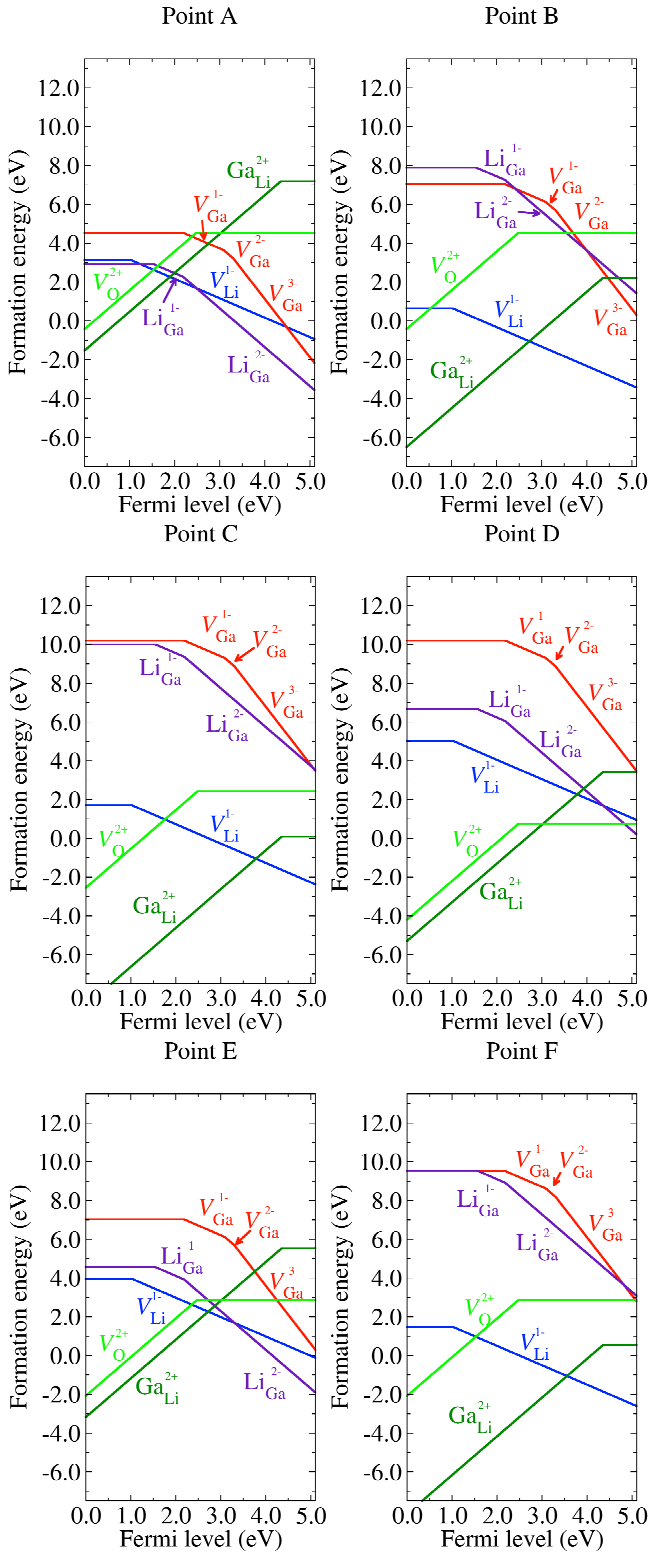

FIG. 3. Energies of formation of various defects in $LiGaO_2$ for chemical potential conditions identified in Fig. 2.

in compensating the Ga_{Li}^{2+}.

Turning now to the O-vacancies, there are two non-equivalent sites for the oxygen in $LiGaO_2$: on top of Li (O_1) or on top of Ga (O_2). We find that both V_{O1} and V_{O2} are only stable in the neutral and 2+ charge states (with V_{O2} slightly lower in energy than V_{O1}) with the transition level (2+/0) at 2.48 eV above the VBM or 2.62 eV below the CBM. This is a quite deep donor level and indicates that the vacancy is also a negative U center. In Fig. 5 one can see that also in this case the relaxations are strongly charge-state dependent. This figure shows the relaxations near a V_{O2} but similar results hold for V_{O1}. In the neutral charge state, the Ga move inward, while the Li move outward. In the 2+ state both move strongly outward. This is similar to the V_O in ZnO[15,28] although the level is here even deeper and close to mid gap. We find that the V_O^{2+} energy of formation is negative for Fermi levels close to the VBM for points C, D, E, F. They become positive for the O-rich limits (A, B). Its energy of formation is always higher than that of the Ga_{Li}^{2+} and thus it is not expected to play a significant role in the charge balance.

Using the charge neutrality condition between free electron concentration $n_e(T, \epsilon_F)$, free hole concentration $n_h(T, \epsilon_F)$ and the various defect concentrations,

$$c(D^q; T, \epsilon_F) = N_D g(q) e^{-(E_f(D^q, \epsilon_F=0)+q\epsilon_F)/k_B T} \qquad (6)$$

where N_D is the number of available sites per cm^3 and $g(q)$ a degeneracy factor depending on the charge state, we can find the equilibrium Fermi level and the defect concentrations for a given temperature following the procedure of Ref.26. For the electron and hole concentrations we use a parabolic band with effective density of states masses $m_e^* \approx 0.4$ and $m_h^* \approx 1.8$ (as obtained from the calculate hybrid functional band structure and averaging over directons.) For a temperature of $T = 1500$ K close to the growth temperature, we find that under chemical potential conditions C, the equilibrium Fermi level is $\epsilon_F = 3.815$ eV, close to the intersection of the V_{Li}^{1-} and Ga_{Li}^{2+}. The electron concentration $n_e = 6 \times 10^{13}$ cm^{-3} but the $[V_{Li}^{-1}] = 2[Ga_{Li}^{2+}] = 1.0 \times 10^{26}$ cm^{-3} are unrealistically high. This is related to the energies of formation of the main defects Ga_{Li} and V_{Li} being negative for the equilibrium Fermi level. For point E, the equilibrium Fermi level position is closer to mid gap, $\epsilon_F = 2.75$ eV with $[Ga_{Li}^{2+}] = 3.7 \times 10^{14}$, $[V_{Li}^{-1}] = 7.22 \times 10^{14}$ and $[Li_{Ga}^{2-}] = 1 \times 10^{13}$ cm^{-3}, $[V_O^{2+}] = 5 \times 10^{12}$ cm^{-3}. So, in this case the concentrations of defects are much smaller and the Ga_{Li}^{2+} is still mostly compensated by V_{Li}^{-1} but partially also by Li_{Ga}^{2-}. The electron concentration at $n_e = 3.2 \times 10^{12}$ cm^{-3} is then only slightly higher than the hole concentration $n_h = 1.6 \times 10^{11}$ cm^{-3} but both free carrier concentrations are in fact negligible under both chemical potential conditions considered. Even under the most Ga-poor conditions (point A), Ga_{Li}^{2+} is the dominant defect and is compensated mostly by V_{Li}^{1-}. In this case, $\epsilon_F = 1.92$ eV is closest to the VBM and the ma-

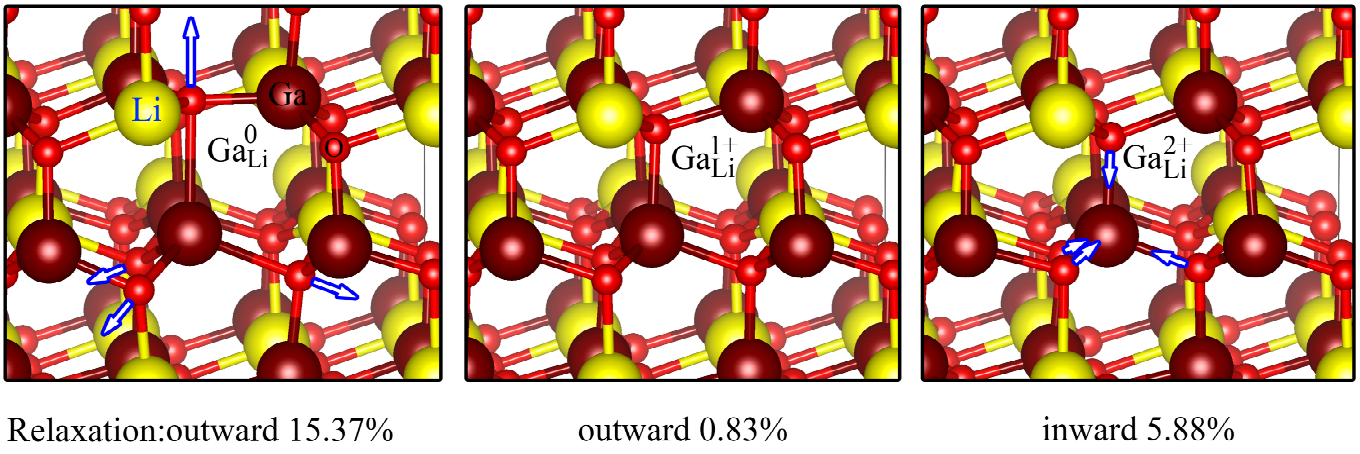

FIG. 4. Structural relaxation for Ga_{Li} in different charge states. Small spheres are oxygen, large red are Ga and yellow are Li. The arrows indicate qualitatively the direction of the displacements away from the perfect crystal positions of the atoms near the defect.

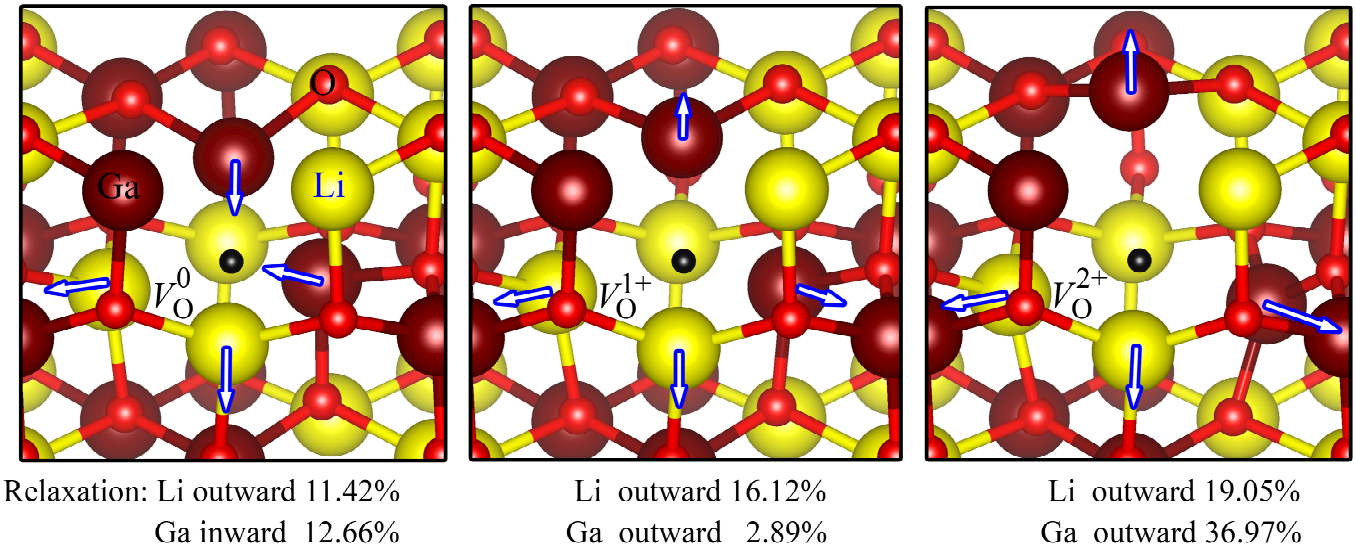

FIG. 5. Structural relaxation for V_{O2} in different charge states. Small spheres are oxygen, large red are Ga and yellow are Li. The arrows indicate qualitatively the direction of the displacements away from the perfect crystal positions of the atoms near the defect. The black dot indicates the vacancy site.

terial would then be slightly p-type with $n_h = 9.7 \times 10^{13}$ cm^{-3}.

TABLE II. Transition levels $\varepsilon(q, q')$ in eV relative to the VBM

Defect	q, q'	$\varepsilon(q, q')$
V_{Li}	(0/1-)	1.03
V_{Ga}	(0/1-)	2.18
	(1-/2-)	3.09
	(2-/3-)	3.31
Li_{Ga}	(0/1-)	1.55
	(1-/2-)	2.19
Ga_{Li}	(0/2+)	4.36
V_O	(0/2+)	2.48

It is instructive to compare the defect physics in this system to that in II-IV-N_2 semiconductors like $ZnGeN_2$,[26]. The similarity is that in both cases, the antisites play a crucial role. However, the dependence on chemical potentials of the elements is more important here because a wider region of stability occurs. Furthermore the Ga_{Li} antisite is here not a shallow but a deep donor and is thus not expected to lead to unintentional n-type doping. This is consistent with the insulating behavior of $LiGaO_2$. However, it does not exclude the possibility of n-type doping by Si or Ge or Sn which will be studied separately.

The main defect transition levels in the gap are summarized in Table II and in Fig. 6.

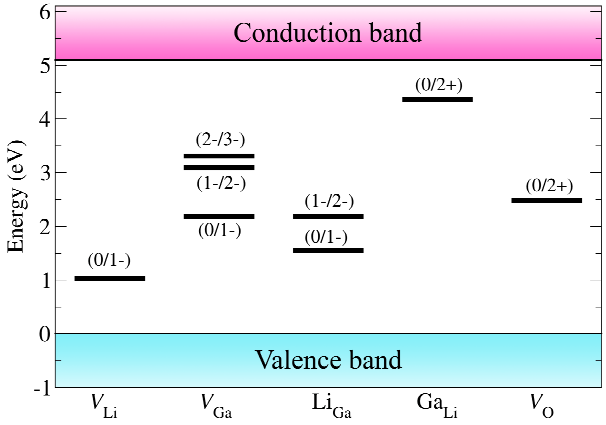

FIG. 6. Defect transition levels in $LiGaO_2$.

IV. CONCLUSIONS

In this paper we have studied the native defects in $LiGaO_2$. We find that the relative energy of formation of vacancies and antisites depends strongly on the chemical potential conditions. The Ga_{Li} antisite is a dominant donor defect. However, it has a rather deep $2+/0$ donor level and is a negative U center. It is thus not expected to lead to significant n-type doping. It furthermore becomes compensated mostly by V_{Li}^{1-} and in part by Li_{Ga}^{2-} depending on how rich the system is in Li. The V_O is found to be an even deeper double donor negative U center. The defect transition levels are all relatively deep in to the gap with no truly shallow levels.

ACKNOWLEDGMENTS

The work at CWRU was supported by the U.S. National Science Foundation under grant No. 1755479. The work at Kasetsart was supported by Kasetsart University Research and Development Institute (KURDI).

[1] K. Sasaki, M. Higashiwaki, A. Kuramata, T. Masui, and S. Yamakoshi, "MBE grown Ga2O3 and its power device applications ," J. Cryst. Growth **378**, 591 – 595 (2013), the 17th International Conference on Molecular Beam Epitaxy.

[2] A. J. Green, K. D. Chabak, E. R. Heller, R. C. Fitch, M. Baldini, A. Fiedler, K. Irmscher, G. Wagner, Z. Galazka, S. E. Tetlak, A. Crespo, K. Leedy, and G. H. Jessen, "3.8-MV/cm Breakdown Strength of MOVPE-Grown Sn-Doped β -Ga2O3 MOSFETs," IEEE Electron Device Letters **37**, 902–905 (2016).

[3] M. Marezio, "The crystal structure of $LiGaO_2$," Acta Crystallographica **18**, 481–484 (1965).

[4] T. Ishii, Y. Tazoh, and S. Miyazawa, "Single-crystal growth of LiGaO2 for a substrate of GaN thin films," J. Crystal Growth **186**, 409 – 419 (1998).

[5] J. T. Wolan and G. B. Hoflund, "Chemical alteration of the native oxide layer on LiGaO2(001) by exposure to hyperthermal atomic hydrogen," J. Vac. Sci. Tech. A **16**, 3414–3419 (1998).

[6] N. W. Johnson, J. A. McLeod, and A. Moewes, "The electronic structure of lithium metagallate," Journal of Physics: Condensed Matter **23**, 445501 (2011).

[7] I. Ohkubo, C. Hirose, K. Tamura, J. Nishii, H. Saito, H. Koinuma, P. Ahemt, T. Chikyow, T. Ishii, S. Miyazawa, Y. Segawa, T. Fukumura, and M. Kawasaki, "Heteroepitaxial growth of β-$LiGaO_2$ thin films on ZnO," Journal of Applied Physics **92**, 5587–5589 (2002).

[8] C. Chen, C.-A. Li, S.-H. Yu, and M. M. Chou, "Growth and characterization of β-$LiGaO_2$ single crystal," Journal of Crystal Growth **402**, 325 – 329 (2014).

[9] A. Boonchun and W. R. L. Lambrecht, "Electronic structure, doping, and lattice dynamics of $LiGaO_2$," in *Oxide-based Materials and Devices II*, Proceedings of SPIE, Vol. 7940, edited by F. H. Terani, D. C. Look, and D. J. Rogers (2011) p. 79400N.

[10] T. Omata, K. Tanaka, A. Tazuke, K. Nose, and S. Otsuka-Yao-Matsuo, "Wide band gap semiconductor alloy: $x(LiGaO_2)_1/2$-(1-x)ZnO," J. Appl. Phys. **103**, 083706 (2008).

[11] T. Omata, M. Kita, K. Nose, K. Tachibana, and S. Otsuka-Yao-Matsuo, "Zn2LiGaO4, Wurtzite-Derived Wide Band Gap Oxide," Jpn. J. Appl. Phys. **50**, 031102 (2011).

[12] S. Nanamatsu, K. Doi, and M. Takahashi, "Piezoelectric, Elastic and Dielectric Properties of $LiGaO_2$," Japanese Journal of Applied Physics **11**, 816–822 (1972).

[13] S. N. Gupta, J. F. Vetelino, V. B. Jipson, and J. C. Field, "Surface acoustic wave properties of lithium gallium oxide," Journal of Applied Physics **47**, 858–860 (1976).

[14] A. Boonchun and W. R. L. Lambrecht, "First-principles study of the elasticity, piezoelectricity, and vibrational modes in $LiGaO_2$ compared with ZnO and GaN," Phys. Rev. B **81**, 235214 (2010).

[15] A. Boonchun and W. R. L. Lambrecht, "Critical evaluation of the LDA+U approach for band gap corrections in point defect calculations: The oxygen vacancy in ZnO case study," Phys. Stat. Solidi (b) **248**, 1043–1051 (2011).

[16] J. Heyd, G. E. Scuseria, and M. Ernzerhof, "Hybrid functionals based on a screened Coulomb potential," J. Chem. Phys. **118**, 8207–8215 (2003).

[17] J. Heyd, G. E. Scuseria, and M. Ernzerhof, "Erratum: "Hybrid functionals based on a screened Coulomb potential" [J. Chem. Phys. **118**, 8207 (2003)]," J. Chem. Phys. **124**, 219906 (2006).

[18] `https://www.vasp.at/`.

[19] G. Kresse and J. Furthmiiller, "Efficiency of ab-initio total energy calculations for metals and semiconductors using a plane-wave basis set," Computational Materials Science **6**, 15–50 (1996).

[20] P. E. Blöchl, "Projector augmented-wave method," Phys. Rev. B **50**, 17953–17979 (1994).

[21] G. Kresse and D. Joubert, "From ultrasoft pseudopotentials to the projector augmented-wave method," Phys. Rev. B **59**, 1758–1775 (1999).

[22] C. Freysoldt, B. Grabowski, T. Hickel, J. Neugebauer, G. Kresse, A. Janotti, and C. G. Van de Walle, "First-principles calculations for point defects in solids," Rev. Mod. Phys. **86**, 253–305 (2014).

[23] C. Freysoldt, J. Neugebauer, and C. G. Van de Walle, "Fully *Ab Initio* finite-size corrections for charged-defect supercell calculations," Phys. Rev. Lett. **102**, 016402 (2009).

[24] J. A. Pople, M. Head-Gordon, D. J. Fox, K. Raghavachari, and L. A. Curtiss, "Gaussian-1 theory: A general procedure for prediction of molecular energies," The Journal of Chemical Physics **90**, 5622–5629 (1989).

[25] K. Reuter and M. Scheffler, "Composition, structure, and stability of RuO_2(110) as a function of oxygen pressure," Phys. Rev. B **65**, 035406 (2001).

[26] D. Skachkov, A. Punya Jaroenjittichai, L.-y. Huang, and W. R. L. Lambrecht, "Native point defects and doping in $ZnGeN_2$," Phys. Rev. B **93**, 155202 (2016).

[27] D. Skachkov and W. R. L. Lambrecht, "Native interstitial defects in $ZnGeN_2$," Phys. Rev. Materials **1**, 054604 (2017).

[28] A. Boonchun and W. R. L. Lambrecht, "Electronic structure of defects and doping in ZnO: Oxygen vacancy and nitrogen doping," Phys. Stat. Solidi (b) **250**, 2091–2101 (2013).